From Benchtop to Field: Calibration and Hardware Optimization of a Low-Power Wireless Potentiostat

1st Matt Whispell
ECE Department
Clarkson University
Potsdam, NY, US
whispemr@clarkson.edu

2nd Zachary Thornton
ECE Department
Clarkson University
Potsdam, NY, US
thorntzm@clarkson.edu

3rd Masudul Imtiaz
ECE Department
Clarkson University
Potsdam, NY, US
mimtiaz@clarkson.edu

***Abstract*—Current lab-grade electrochemical sensors (aka potentiostats) are bulky, expensive, and require specialized lab setups. Along with this, there is a need for wireless technology in these sensors for use in environmental monitoring, wearable devices, and medical diagnostics. To solve this problem, we use the TI LMP91000 analog front end in combination with a SiLabs EFR32BG24 microcontroller, which supports Bluetooth 5.3. This sensor had already been developed, and introductory validating experiments were conducted, but it has not been tested in the field on a variety of chemical solutions [1]. Furthermore, a calibration curve has not been created to fit data from the device to known concentrations, which prevents the sensor from accurately measuring minute concentrations in solution.**

***Index Terms*—sensor, detection, electrochemical, embedded**

I. Introduction

This sensor is an open-source project that is still in active development. This setup uses the DAC (Digital to Analog Converter) on the EFR32 microcontroller to direct the LMP91000 to apply a voltage waveform. A TIA (TransImpedance Amplifier) in the LMP91000 measures the current that flows through the electrode as a result of the voltage applied to it. Using the changes in time, voltage, and current, the concentration of the contaminant of interest can be determined.

The LMP91000 is a feature-rich AFE, meaning that it can be complex to implement custom sensors with that frontend. For example, it is necessary to communicate with the sensor over i2c (inter-integrated circuit protocol) to configure how voltage waveforms will be applied and how the current flowing will be read back. Roadblocks were encountered here, as the behavior of the MENB (active low enable pin) is poorly documented in the LMP91000 datasheet [2]. The datasheet claims that the MENB pin can be held low for the entire use of the sensor, but it was discovered that this prevents i2c communications from working properly. This is just one example of the many speedbumps that may be encountered when working on a custom sensor project as discussed in this paper.

Before this data coming from the sensor will be useful, it is necessary to create a calibration curve that compares data from this sensor to known values, allowing all future data to be fit to that calibration curve. To do this, it is first necessary to ensure that all software bugs are fixed in the sensor's firmware, then data can be collected. To ensure that data from our sensor is close enough in waveform, it will be necessary to have a tool that can easily compare electrochemical experiments. In this case, it is easier to create a custom program for this in Python.

SDIP-REU

II. Objectives

Since the bulk of development has been completed, the aim of this research is to compare data from this sensor to that of lab-grade equipment. This process will involve testing and revising the sensor platform to ensure experimental results for cyclic voltammetry (CV), square wave voltammetry (SWV), differential pulse voltammetry (DPV), and chronoamperometry (CA) are accurate within a reasonable degree. Part of this process involves solving hardware and software issues that arise to allow for the chemistry department to reliably run experiments in the future. Once this phase is completed, it is necessary to apply electrochemical experiments in the field with as many solutions as possible to ensure the sensor functions properly in a wide range of environments. Finally, once that is done, these results should be numerically evaluated to ensure that this sensor will provide comparable detection characteristics to lab-grade equipment while in the field.

III. Hardware Design Issues

A. Virtual Ground Referencing

The LMP91000 AFE utilizes a single ended power input, meaning that it requires 3.3V and ground to operate. In its operation, it is necessary to be able to drive the V_{out} pin above and below ground. This is not usually possible with a single ended power input, so the LMP91000 uses a virtual ground [2]. This allows the output of the device to go below the virtual ground, effectively creating a negatively biased voltage. The virtual ground is determined by the voltage applied to the V_{ref} pin, and the zero % register set through i2c communication.

When reading voltages from the LMP91000, it is imperative that they are taken relative to the virtual ground generated by the chip, not relative to circuit ground. Furthermore, excess care must be taken when measuring voltages in the circuit. When using an oscilloscope to measure electrode potential and current readings, the act of taking a measurement was observed to effect the outcome of an experiment. The cause of this issue is in shorting the virtual ground generated to

the circuit ground, breaking down the feedback loop inside the LMP91000 and causing erroneous behavior. The electrical cause of this issue stems from the fact that the measurement equipment and the PC being used to power the board during debugging sharing a common ground at the wall. The PC is grounded, which in turn grounds the USB ports on the PC, which supplies the ground to the potentiostat board. This same outlet powers the oscilloscope, where the ground of each probe is connected to the circuit ground. This means that the oscilloscope ground probe directly connects the virtual ground to the circuit ground, causing this issue.

Upon encountering this problem, two solutions were devised. In the first, the math function of the oscilloscope is utilized. By taking two ground-referred measurements (with circuit ground connected to the ground clip) and doing a subtraction operation on them on the scope, it is possible to reconstruct the same measurement that can be taken incorrectly with one probe, correctly with two probes. The second solution to this issue is even simpler. Since the custom PCB was designed with portability in mind, it has the necessary hardware to support being powered by a battery. By powering the potentiostat from this battery, the board has been isolated from wall ground and taking measurements virtual-ground-referred is valid. Note that if a different setup didn't have battery capability, a laptop running on battery powering the board through the debug connector can also successfully recreate this workaround.

B. Inaccurate Onboard Clock Source

One feature of this sensor platform is that it can keep track of time and timestamp experimental results without being connected to a time server. This is currently achieved with an onboard LFRCO (Low-Frequency RC Oscillator) which is a type of clock source that is quite inaccurate over time with drift adding up quickly. Along with this, the LFRCO is affected by temperature variations, leading to the onboard timer to lose about 27s/hr at room temperature. This means the current design will lose 10.8min of accuracy over a 24hr timespan. That is not acceptable for an accurate time measurement.

One potential fix of this problem would be to run the LFRCO in precision mode. This would make the clock source more accurate, but it has a major drawback. Precision mode cannot be used in EM4 (Energy Mode 4) sleep [3], meaning time could not be kept when using the lowest energy consumption state. To remedy this problem, during the hardware revision, a 32.768kHz LFXO (Low-Frequency Crystal Oscillator) was connected to the MCU to allow the device to use hardware dividers to obtain a 1Hz clock (because 32,768 is a multiple of two). This solution is low cost (only adding about $0.70 per board), and barely increases design complexity.

IV. Hardware Design Fixes

Due to the missing virtual ground connection, and the need for the LFXO, it was necessary to make hardware design changes and order another board revision. This can be a lengthy process from fixing the design, to ordering boards and parts, to assembly and testing. To continue the research with higher quality data, it would be necessary to find a workaround that allows the current hardware to take the virtual-ground referred measurement.

Luckily, there is a simple workaround that allows for the virtual ground network to be connected to an analog capable pin on the MCU. The board design contains debugging pads which interface with a pogo pin connector, allowing the device to be programmed over a SWD (Serial Wire Debug) connection. By setting up an OTA (Over The Air) bootloader, it is possible to upload firmware to the device over Bluetooth after an initial programming over the SWD connector. Since firmware is now uploaded over Bluetooth, it is possible to reuse one of the debug pads as an analog input for the negative end of the ADC. Conveniently, the virtual ground net is also exposed on a pad on the board, the C1 pad for adding extra feedback impedance which is currently unused. This allows for connection of this net to the MCU to make a relative measurement. Fig. 1 shows the internal hardware of the LMP91000 that makes this workaround possible, and Fig. 2 highlights the fix area.

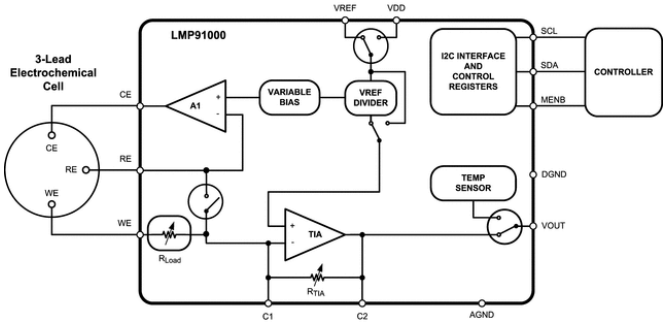

Fig. 1: Block diagram of internal circuitry of the LMP91000.

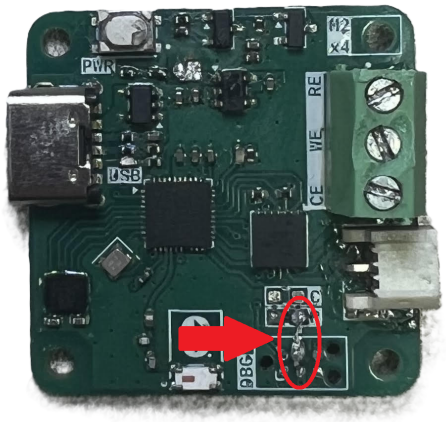

Fig. 2: Connection between C1 and a debug header pin.

V. Software Design Issues

A. Communicating with the LMP91000

The LMP91000 is a feature-rich AFE, which comes at the cost of increased complexity. This chip uses i2c communication, requiring registers to be written with the proper value. When interfacing with the EFR32, some considerations must be taken. Firstly, the i2c address of the LMP must be entered into the firmware shifted left by one bit. This means that the address 0x48 from the datasheet becomes 0x90. Once the proper address is in place, the behavior of the MENB (enable) pin must be considered. Although the datasheet claims that if only one LMP is on the bus that the MENB line can be held low (to enable the chip constantly). This has not appeared to be the case here, and asserting and deasserting the MENB pin every use seemed to be necessary here.

B. Estimating the virtual ground voltage

To reiterate, the virtual ground of the LMP91000 is governed by the following equation:

$$V_{gnd} = V_{ref} * Bias\% \tag{1}$$

The need for mV precision introduces the need to vary V_{ref}, leading to the virtual ground constantly changing throughout an experiment. One theory to circumvent need for the board revision discussed previously was that it is possible to calculate the virtual ground voltage on the MCU, as V_{ref} is known and $Bias\%$ is also known. Upon testing this theory in the program, it was found that this calculation is not close enough to the real V_{gnd}. At worst, there was found to be $\approx 200mV$ of difference between the calculated and real value, likely due to transients in the virtual ground circuitry from constant change of V_{ref}. This showed that estimation of this value is not sufficient for the accuracy required of this sensor, and proved that a hardware revision was necessary.

VI. Software Design Fixes

Fixing the i2c address and MENB behavior of the sensor are simple changes that only involve small software changes. It was only necessary to shift the i2c address by one bit, and to ensure that MENB is being asserted at the beginning of every i2c transfer, and that it is being deasserted at the end.

As mentioned above, it is not possible to estimate the virtual ground voltage, as the calculation is not accurate enough to the real-world transients. While it was considered to make a look up table for these virtual ground voltages, if 5mV resolution was desired, to account for all biases, it would take over 5,000 table entries that would have to be written in the program memory, wasting space and time. This leaves the hardware workaround as the only way to properly read the current from the TIA. To account for this fix in software, a new bootloader would need to be uploaded, with advanced capability. Not only would the device need to support OTA firmware updates, but it would also need OTA debugging to allow the firmware changes to be debugged. This process was simple, only requiring a "Bootloader Application Interface" software component to be installed in the Simplicity Studio 6 project, and upon reflashing the board the OTA bootloader was in place. OTA debugging required adding a Bluetooth service for debugging, and creation of a Bluetooth debug program in Python that prints all debug messages to a terminal on a laptop or PC. Only once these two crucial steps are completed, it was possible to reconfigure the software to utilize one of the SWD pins as the negative input of the ADC.

VII. PCB Redesign

A. Adding the virtual ground reading

During the consideration of the hardware changes to be made, KickStat was used as an influence . The KickStat firmware separately reads V_{out} and C1 from the LMP91000, then subtracts C1 from V_{out} [4]. Since the EFR32 on-chip ADC supports differential readings, it made more sense here to take a true differential measurement. This means that V_{out} will be the positive input and C1 will be the negative input. This method allows the two pins to be compared simultaneously, which helps when there is a quickly changing transient involved, and it cuts down on quantization error, as this method performs only one ADC reading instead of two. When adding the virtual ground connection, it was necessary to take care in the pins being utilized, as the EFR32 has hardware quirks that will require another hardware revision if not considered carefully. One such quirk is that due to the analog bus routing system, the positive ADC input must be connected to an even pin, and the negative input must be connected to an odd pin [3]. Fig. 3 shows the added trace:

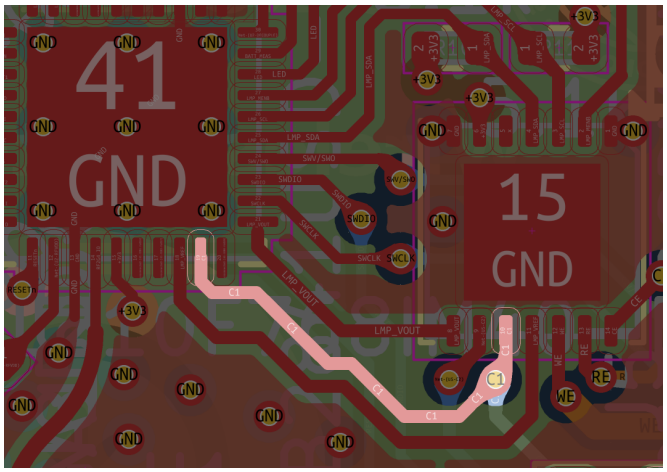

Fig. 3: New C1 trace on the PCB to read the virtual ground voltage.

Note how V_{ref} has been moved to a different pin to open an area for the C1 trace to be routed without any vias, for signal integrity and minimal trace length. Furthermore, C1 connects to an odd pin so that it may be used as a negative ADC input.

B. Adding the LFXO

Due to the inaccuracy of the LFRCO and impending board redesign, it was decided to add an external LFXO for the MCU

to utilize with it's internal BURTC (back-up real-time clock). The reason the back-up RTC is used is because the main RTC does not work in EM4 sleep. So since the current revision cannot use the main RTC or the high-precision mode of the LFRCO, it makes the most sense to add an LFXO to the board. The EFR32 requires that this LFXO is connected to only PD00 and PD01, no other pin [5]. This presented a slight roadbump, as the battery measurement readout was previously connected to PD00. Rerouting the battery measurement required two additional vias, but was a relatively easy fix. The bigger issue was the space necessary for the crystal, and the requirement for the crystal to be close to the MCU for signal integrity.

Fig. 4 shows where the crystal needed to be placed, and which pins it was necessary to connect to. It is clear from that image that there was not enough space for the crystal to be that close to the board, and it would be necessary to move other components. By moving the USB power LED up and to the right, space was created for the LFXO to be in close proximity to the MCU. Along with this, ground stitching vias were added around the crystal's traces, for further integrity of the clock signal. Fig. 5 highlights where this change was made.

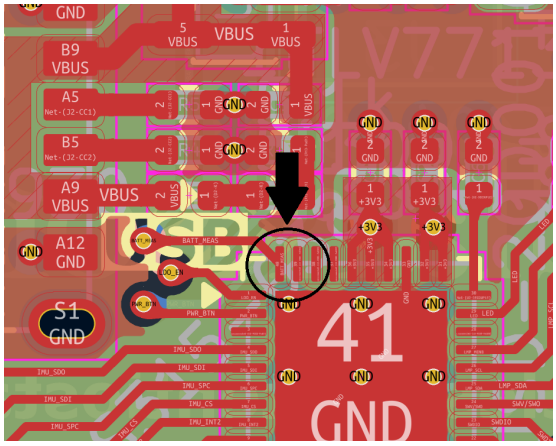

Fig. 4: Previous design with PD00 and PD01 highlighted.

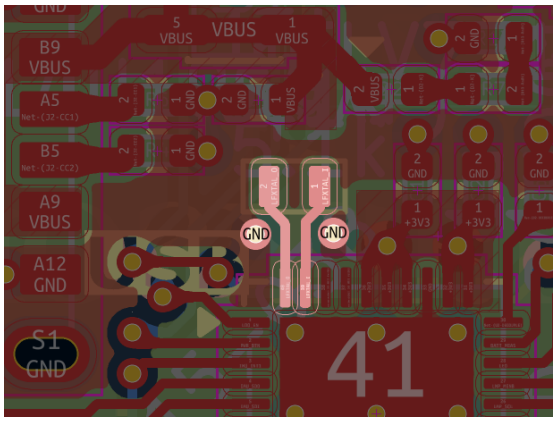

Fig. 5: New design with LFXO added and other components moved.

C. *Better shielding for electrode traces*

The electrode traces are one of the most sensitive parts of the potentiostat circuitry, therefore utmost care must be taken to shield them from EMI (electromagnetic interference). In the previous design of the PCB, these electrode traces were on the top and bottom layers of the board where there is not only more signal and power runs, but exposure to the outside environment. It is theorized that by moving these traces to inner layers of the board, they will be sandwiched between ground planes of the top and bottom layers, essentially creating a faraday cage encasing these traces.

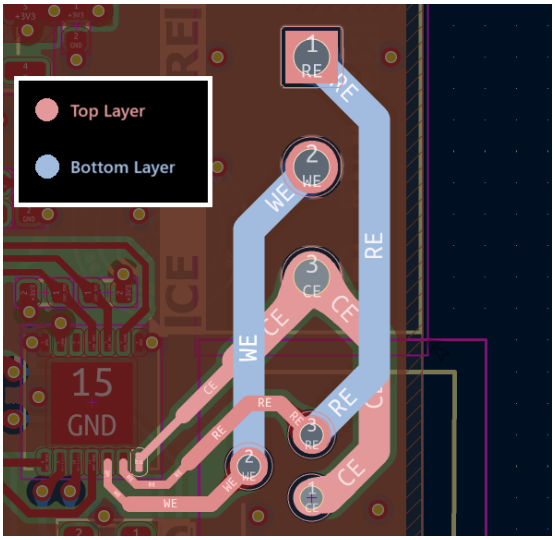

Fig. 6: Previous routing with electrode traces on the top and bottom.

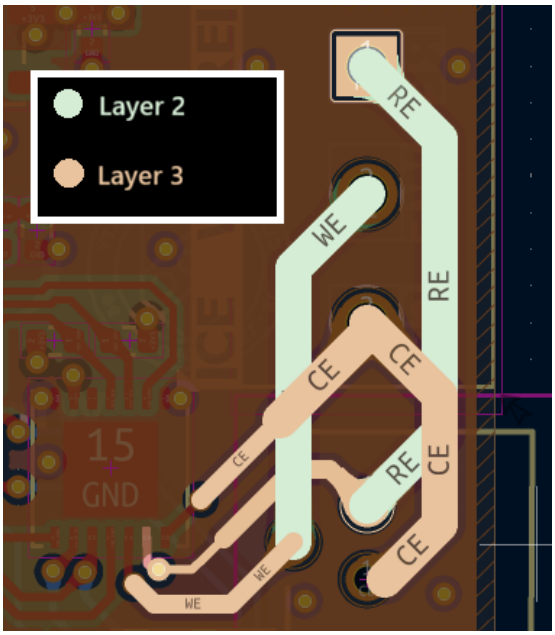

Fig. 7: New routing with electrode traces sandwiched between ground planes.

VIII. Comparing experimental data

A. Creating the tool

In the course of this research, many CV and CA experiments were conducted, and their results exported via the app and saved. To be able to process all these experiments, a custom Python application was created. The application uses MatPlotLib for plotting, Pandas for data analysis, and TKinter for the user interface. The app allows the user to import .csv data from a known good sensor and a sensor in test. The application will automatically detect whether the experiment is a CV, CA, or multipoint CA experiment, and then run the proper analysis. The application will highlight characteristics from each sensor such as anodic and cathodic peak currents and potentials, and also compare the data from the two sensors. It will provide the anodic peak shift and the peak anodic current ratio. To summarize all this data, the application re-interpolates the data to normalize the number of points in both datasets, then performs a mean point-by-point standard deviation calculation. It compares this deviation over the entire experiment to the overall magnitude of the experiment, to provide the percentage overall similarity match. The interface of this application is shown below in Fig. 8.

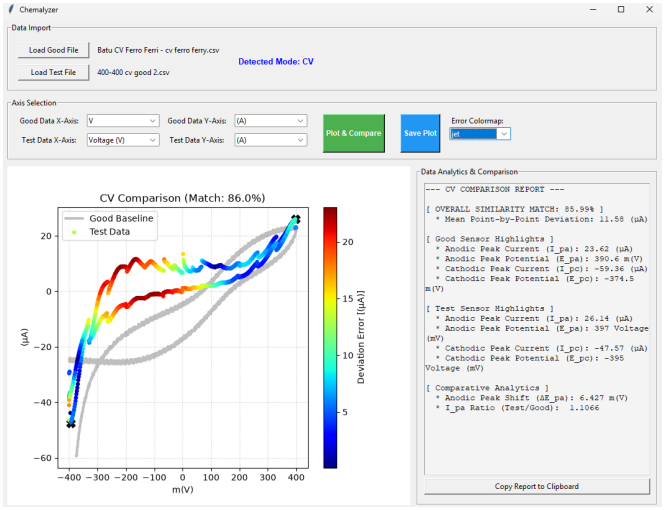

Fig. 8: The Chemalyzer application. CV data is loaded into the app to showcase the functionality

B. Qualitative observations

The deviation error graphing feature of the Chemalyzer app was extremely useful in characterizing which parts of the electrochemical experiment contributed most to overall deviation. It was observed that this sensor frequently struggled to properly react to reducing electrochemical conditions. As the potential applied to the electrode became negative, the response would start out very weak, but become exponentially stronger. This lead to any experiments with electrode potentials of less than about 500mV to drop in current so quickly that the primary oxidation and reduction features of the plot were washed out. For this reason, most of the experiments shown in this paper stay within that potential range.

One theorized cause of this behavior is that the electrodes being used to run experiments are degraded. Since the sensor is still in development and final validation is to come, it is more economical to utilize used electrodes from the chemistry department. The carbon substrate is further degraded on some electrodes compared to others, leading to erroneous data. Most of the experiments compared here were performed with the same electrode on both the lab-grade equipment, and our sensor. Figures 9 & 10 compare multipoint CA experiments from the Sensit Smart PalmSens [6] and our sensor, with the same parameters.

The PBS experiment highlights the enhanced performance of the oxidation pathway, and the muted reduction path is made evident. Our sensor only shows about 1/3 of the reduction response compared to that of the lab-grade potentiostat. As mentioned previously, some of this reduced response may be caused due to electrode quality, but clearly that is not the only problem at play.

The ferro-ferri solution had similar behavior to the PBS experiments, although it more consistently matched peak currents obtained from the lab-grade sensor. The Chemalyzer program also supports analysis of CV experiments. Important qualitative distinctions were also obtained from comparing CV experiments, seen in Figures 11 & 12

The CV result in Fig. 11 is quite poor, and it seems that our sensor has a much stronger overall response to the applied potential. This is an example of two experiments with the exact same parameters but two electrodes of differing quality, leading to a reduced response. It appears that between these experiments, the electrode used in the lab-grade sensor was much more degraded than that in our sensor, leading to the comparatively poor response. This highlights the importance of using the same electrode between platforms, especially if not using fresh electrodes.

A much better result is seen in a CV performed in ferro-ferri with the same parameters, showcased in Fig. 12. While this data is much closer to the lab-grade data, it still leaves more to be desired from this sensor. As seen in previous experiments, the oxidation pathway is extremely close, if not overshooting that of the good data. The reduction path however, does not respond as accurately and remains much lower in absolute current flow.

C. Quantitative observations

The Chemalyzer tool also outputs large amounts of numerical data about each individual curve, and the comparison between the two curves. Going through the metrics Chemalyzer outputs, the first is the overall similarity match. This is a normalized percentage score that indicates how closely the overall shape and magnitude of the two curves match. This acts as an initial pass/fail metric that indicates whether the two experiments are close enough to even be worth comparing. Each experiment type has different metrics. In CV analysis, the tool returns anodic and cathodic peak current, I_{pa} & I_{pc},

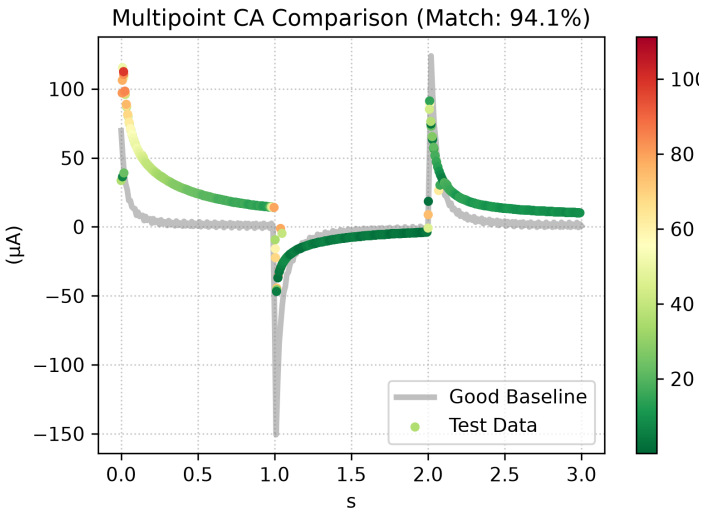

Fig. 9: Comparison results of a 3 point CA with levels 200mV for 1s, -200mV for 1s, and 200mV for 1s. Performed in pH 6.6 PBS

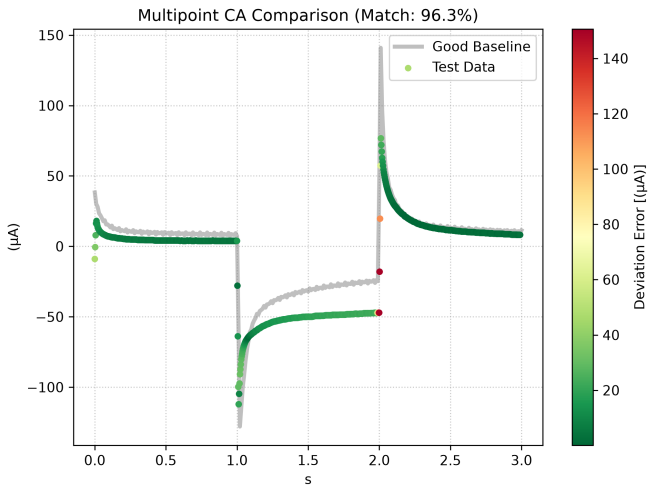

Fig. 10: Comparison results of a 3 point CA with levels 200mV for 1s, -200mV for 1s, and 200mV for 1s. Performed in 5mM ferrocyanide, 5mM ferricyanide, 0.1M KCl solution.

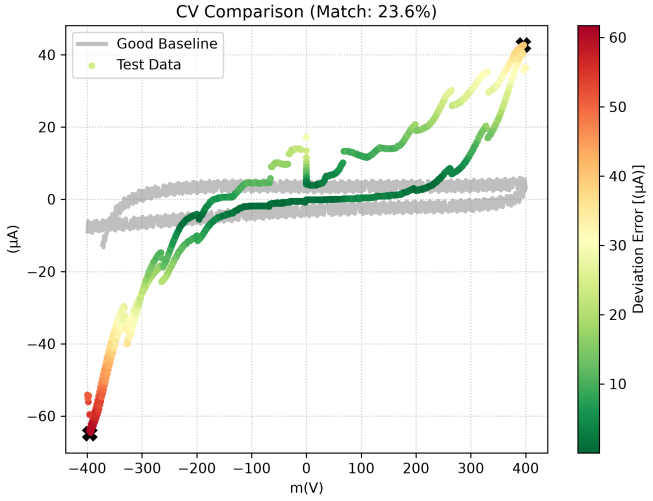

Fig. 11: Comparison results of a CV with vertexes at 400mV and -400mV, with a 100mV/s step rate. Performed in pH 6.6 PBS

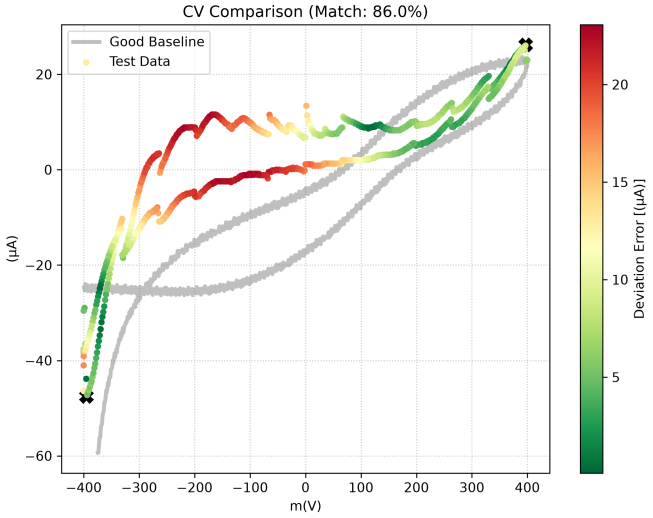

Fig. 12: Comparison results of a CV with vertexes at 400mV and -400mV, with a 100mV/s step rate. Performed in 5mM ferrocyanide, 5mM ferricyanide, 0.1M KCl solution

respectively. The peak current response is governed by the Randles–Sevcik equation [7]:

$$I_p = (2.69 \times 10^5)\, n^{3/2} A D^{1/2} C v^{1/2} \tag{2}$$

where I_p is the peak current (A), n is the number of electrons transferred in the redox event, A is the electroactive surface area (cm^2), D is the diffusion coefficient ($\mathrm{cm}^2\,\mathrm{s}^{-1}$), C is the bulk analyte concentration ($\mathrm{mol\,cm}^{-3}$), and v is the potential scan rate ($\mathrm{V\,s}^{-1}$).

CV experiments also return the anodic peak potential, the voltage potentials where the oxidation and reduction rates are at their peak. These metrics indicate electrochemical reversibility. Furthermore, it returns the anodic peak shift, which is the difference between the baseline E_{pa} and test E_{pa}. Finally, it returns the I_{pa} ratio, which measures the relative sensitivity of the sensors. A ratio of 1.0 indicates identical sensitivity between the two sensors, and values greater than or less than 1.0 indicate a variation in sensor area or loading.

CA returns the peak transient current, which is the initial spike observed after applying the step potential. Higher spikes indicate micro-shorts, and diminished spikes indicate higher contact resistances. The steady state current, I_{ss}, is directly proportional to the analyte diffusion and concentration [7]. The transient current response following a potential step is governed by the Cottrell equation:

$$I(t) = \frac{nFAC\sqrt{D}}{\sqrt{\pi t}}, \tag{3}$$

where $I(t)$ is the current (A), n is the number of electrons transferred in the redox event, F is Faraday's constant ($96{,}485$ C mol^{-1}), A is the active electrode surface area (cm^2), C is the bulk analyte concentration (mol cm^{-3}), D is the diffusion coefficient (cm^2 s^{-1}), and t is the elapsed time (s).

Finally, CA comparisons return the total integrated charge (Q). The total mass of substance deposited or liberated at an electrode during electrolysis is expressed by Faraday's law of electrochemistry [7]:

$$m = \left(\frac{Q}{F}\right)\left(\frac{M}{z}\right) = \frac{ItM}{zF}, \tag{4}$$

where m is the mass of the substance (g), Q is the total electric charge passed (C), F is Faraday's constant ($96{,}485$ C mol^{-1}), M is the molar mass of the substance (g mol^{-1}), z is the valency number of the ion (number of electrons transferred per ion), I is the electric current (A), and t is the total duration of electrolysis (s).

These metrics are crucial in getting useful analyte concentration data from electrochemical experiments. Therefore, ensuring these statistics match between the lab-grade sensor and our sensor is imperative.

The quantitative comparison begins with the multipoint CA experiments in PBS, seen in Fig. 9. The overall similarity match is 97.31%, the mean deviation is $7.119\mu A$, and the steady-state current ratios are 5.94, 2.79, and 4.44, respectively. This shows that these experiments have a good profile match, but our sensor exhibited a higher steady-state current across all potential steps. Furthermore, there is a baseline offset between these experiments, for example in the first step the test sensor reaches a steady state current of $5.736\mu A$ while the lab-grade sensor settles at 966.3nA. This leads to the conclusion that there is parasitic background current or electrode leakage.

The multipoint CA experiment in ferro-ferri seen in Fig. 10 returns slightly better results. The overall similarity is 96.34%, the mean deviation is $9.47\mu A$, and the steady-state current ratios are 0.46, 1.87, and 0.80, respectively. While there is a strong overall shape match, steps 1 and 3 (anodic steps) have a weak response, making 46% and 80% of the reference steady-state current. Conversely, step 2 (cathodic step) causes our sensor to over-respond, generating 1.87x the reference steady-state current. This indicates baseline shifting during multi-cycle experiments.

CV experiments can be compared similarly, but focusing on anodic peak current and peak shift instead. In the CV experiment performed in PBS seen in Fig. 11, the two experiments had wildly different outcomes. Much of this difference can be attributed to using a degraded electrode in the lab-grade sensor experiment, yet it still provides an important view into how the Chemalyzer tool handles poor experiment data. The overall similarity match was only 23.63% here, quickly indicating that these experiments are barely comparable. The mean deviation is $13.83\mu A$, the I_{pa} ratio at 7.19, and an anodic peak shift (ΔE_{pa}) of 6.50mV. The reduced quality of the electrode used in the lab-grade sensor is very evident here, with our sensor producing over 7x higher anodic peak current! This makes it clear that more data should be taken with better matching electrode surface quality.

A much better CV comparison is seen in the ferro-ferri experiment in Fig. 12. Here the overall similarity is 85.99%, the mean deviation $11.58\mu A$, the I_{pa} ratio at 1.11, and (ΔE_{pa}) of 6.43mV. This shows that there is good overall agreement between the two sensors, with an anodic peak current within 10% of the lab-grade sensor. The cathodic response is slightly supressed $I_{pc} = -47.57$ µA vs. -59.36 µA, which points to a small uncompensated resistance or slight reaction sluggishness.

Across all experiment evaluations, our sensor consistently reproduces the overall transient shapes and profile dynamics of the lab-grade reference. It consistently achieved $> 85\%$ to $> 97\%$ profile similarity across valid runs (CV in PBS excluded due to electrode quality affecting results). Overall, our sensor demonstrates strong transient response, but has reduced effective area ($\approx 37\%$ charge loss), elevated leakage currents with some analytes, and exhibits slightly potential-dependent asymmetric kinetics.

IX. Next steps and further research

Now that the virtual ground theory has been confirmed and new boards ordered, the new boards will have to be assembled and tested. It is our hope that the boards with dedicated traces for the virtual ground network will perform even closer to lab-grade potentiostats. The current fix leaves performance on the table with high connection resistance, leading to voltage drop over the length of the trace, muddying the virtual ground reading. Once the new boards are assembled and performing experiments, it will be possible to quantify the increase in experimental quality with the Chemalyzer tool.

Furthermore, our sensor platform will finally be ready for implementation into electrochemical research. This sensor, with its Bluetooth capability is ideal for experiments such as PFAs detection, pesticide detection, sweat biomarker monitoring, and much more. It will be important to use the Chemalyzer tool to compare performance of our sensor and lab-grade sensors in these experimental situations. These experiments commonly use CV as a preparation step for the electrode surface, then use DPV or SWV to detect analyte levels. Therefore, it will be imperative to ensure that those experiments have highly similar characteristics on our sensor and the lab-grade sensor.

References

[1] S. Kukla et al., "Lessons learned from designing a wireless universal electrochemical sensor platform," *IEEE Sensors Journal*, 2022.

[2] Texas Instruments, "LMP91000 Configurable AFE Potentiostat for Low-Power Chemical-Sensing Applications," Datasheet SNAS506I, Rev. I, May 2013 [Revised 2020].

[3] Silicon Laboratories, "EFR32xG24 Wireless SoC Reference Manual," Rev. 1.1, 2024.

[4] O. S. Hoilett et al., "Kickstat: A coin-sized potentiostat for high-resolution electrochemical analysis," *Sensors*, vol. 20, no. 8, p. 2407, Apr. 2020. doi: 10.3390/s20082407.

[5] Silicon Laboratories, "EFR32BG24 Wireless SoC Family Data Sheet," Rev. 1.1, Nov. 2024.

[6] PalmSens BV, “Sensit Smart: Smartphone Potentiostat Technical Specifications,” Product Description Sheet, 2019.
[7] A. J. Bard and L. R. Faulkner, *Electrochemical Methods: Fundamentals and Applications*, 2nd ed. New York: John Wiley & Sons, 2001.